Neutrino flavor evolution in high-flux astrophysical environments

J. Carlson,[1] A. Roggero,[2,3] and Duff Neill[1]

[1]*Theoretical Division, Los Alamos National Laboratory, Los Alamos, New Mexico, 87545, USA*
[2]*Dipartimento di Fisica, University of Trento, via Sommarive 14, I–38123, Povo, Trento, Italy*
[3]*INFN-TIFPA Trento Institute of Fundamental Physics and Applications, Trento, Italy*

(Received 13 May 2026; accepted 25 September 2026; published 10 November 2026)

We examine neutrino evolution in astrophysical environments where the neutrino flux is very large, including core-collapse supernovae and neutron star mergers. In these environments, the neutrino-neutrino and neutrino-antineutrino interactions are crucial. We include nonforward scattering of neutrinos and antineutrinos in a semiclassical treatment. Because of the large scale of neutrino momenta (2–10 MeV), the quantum evolution problem can be treated as a sum over incoherent paths in the momentum and flavor of each neutrino. The phases between different neutrinos are essentially random because of the large kinetic terms. Momentum is conserved at each vertex, and important flavor symmetries are retained. Dynamics in the many-body neutrino system enable rapid equilibration in the energy and angular distributions of all flavors, and an equilibration of products of neutrino and antineutrino densities for each flavor at either large or zero background matter density. We also describe the evolution at moderate densities where the mass eigenstates differ for neutrinos and antineutrinos, and with time-varying background matter densities. The evolution maintains relevant symmetries and reduces to standard Mikheyev-Smirnov-Wolfenstein oscillations in the appropriate limits. The rapid equilibration in energy and flavor can significantly impact energy deposition and nucleosynthesis in high-flux astrophysical environments, and potentially flavor energy relations in terrestrial supernovae neutrino observations.

DOI: 10.1103/dds1-t759

I. INTRODUCTION

For many astrophysical environments like the Sun, neutrino flavor evolution is well understood through single-particle evolution and the Mikheyev-Smirnov-Wolfenstein (MSW) mechanism [1,2]. In environments with large neutrino fluxes, however, neutrino-neutrino and neutrino-antineutrino interactions can play a role [3–7] (see also Refs. [8–10] for recent reviews). Here we consider the evolution of neutrino flavor, including kinetic terms (neutrino momenta), the vacuum plus matter (MSW) one-body interactions, and two-neutrino interactions. A complete quantum treatment of this problem for large systems of neutrinos and antineutrinos is prohibitive due to the large number of quantum amplitudes involved and the long time evolution required. This major challenge has motivated efforts to explore the use of approximate many-body techniques [11–41] and, in recent years, also quantum computing [42–51].

In this work, we develop a semiclassical treatment analogous to standard classical mechanics but including the time evolution of the momenta and flavor amplitudes for each neutrino. The many-body quantum system equilibrates at a similar rate to the forward scattering Hamiltonian, as discussed below. The semiclassical approximation ignores interference between one insertion of the two-neutrino interaction and the next insertion involving one of the same particles. Since the kinetic terms in the Hamiltonian are a factor of 10^{10} larger than the two-body terms, the phase will oscillate extremely rapidly between insertions and this approximation should be very accurate. The semiclassical approximation treats the magnitude of the insertions exactly. This is verified in comparisons of full quantum and semiclassical calculations. Though the actual final state is highly entangled, simple one-body observables can be accurately evaluated as averages over trajectories in this semiclassical approach.

We assume the fermionic nature of the neutrinos is not important, as in Ref. [52]. Assuming an average energy of 7.5 MeV, a flux of 10^{53} erg/ sec, a radius of 50 km, and a dominance of neutrinos over antineutrinos, the occupancy of single-particle neutrino states below 10 MeV is only about ten percent. These conditions give an average distance of roughly 1 cm at 50 km between neutrino-neutrino interactions impacting a specific pair. At these

Published by the American Physical Society under the terms of the Creative Commons Attribution 4.0 International license. Further distribution of this work must maintain attribution to the author(s) and the published article's title, journal citation, and DOI. Funded by SCOAP³.

energies the nondegenerate nature of the neutrinos implies that Fermi statistics would be important only when the individual flavor states approach degenerate conditions. We discuss the equilibration rate in more detail below.

II. HAMILTONIAN

We consider a system of N neutrinos at a finite density described by the Hamiltonian of the form

$$H = H_0 + H_{1,v} + H_{1,m} + H_2. \tag{1}$$

The Hamiltonian is written in the basis of products of single-particle states, where each neutrino has a definite flavor state χ_i and a definite momentum $\mathbf{k}_i$.

The first term H_0 is the leading-order kinetic term

$$H_0 = \sum_{i=1}^{N} |\mathbf{k_i}| \tag{2}$$

for massless neutrinos, where i runs over the N neutrinos. The H_1 terms are the vacuum ($H_{1,v}$) and matter terms ($H_{1,m}$) well studied for solar neutrinos and extraterrestrial neutrinos passing through the earth, for example. They are also being studied in large experimental campaigns using accelerator neutrinos to determine the mass hierarchy and potential CP violation in the neutrino sector. Finally, the last term H_2 describes the neutral-current-mediated interaction between neutrinos.

In this paper, we consider Dirac neutrinos with a normal mass ordering and no CP violation. Extensions to Majorana neutrinos with CP violation are an intriguing subject for future study. With these choices, the numbers of neutrinos and antineutrinos are individually conserved.

The two-neutrino interactions are flavor operators times a vertex function of momenta nearly independent of the magnitude of momentum transfer $\mathbf{q}$ (since it is a very short-range interaction) times a function of the angles of incoming and outgoing momenta. The interactions operate on the entire flavor space of each neutrino, with a constant term plus a flavor exchange term (for neutrino-neutrino interactions) or a constant plus a term coupling a neutrino-antineutrino pair with the same initial flavor to final states of the other flavors. This is the same Hamiltonian studied in Ref. [38]. Additionally, we use semiclassical methods to address a large number of neutrinos, study cases with different background matter profiles, and address the impact of a mixture of neutrinos and antineutrinos.

We express a general neutrino state with a fixed momentum in a coupled flavor-momentum basis as follows:

$$|\psi_m(i)\rangle = \sum_{f=1}^{N_f} \chi_{mf}(i)|f\rangle \otimes |\mathbf{k}_m\rangle, \tag{3}$$

where states $|f\rangle$ form a basis for the $SU(N_f)$ flavor space (i.e., for $N_f = 3$ these are $|\nu_e\rangle$, $|\nu_\mu\rangle$, and $|\nu_\tau\rangle$). The coefficient matrix $\chi_{mf}(i)$ stores the flavor amplitudes of the single-particle state. For antineutrinos, we similarly write

$$|\bar{\psi}_m(i)\rangle = \sum_{f=1}^{N} \bar{\chi}_{mf}(i)|\bar{f}\rangle \otimes |\mathbf{k}_m\rangle. \tag{4}$$

A general many-body state with N_ν neutrinos and $N_{\bar{\nu}}$ antineutrinos can be expressed as a linear combination

$$|\Psi\rangle = \sum_n \alpha_n |\phi_n\rangle, \tag{5}$$

where the states $|\phi_n\rangle$ are product states of the form

$$|\phi_n\rangle = \bigotimes_{i=1}^{N_\nu} |\psi_{m_n}(i)\rangle \bigotimes_{j=1}^{N_{\bar{\nu}}} |\bar{\psi}_{\bar{m}_n}(j)\rangle, \tag{6}$$

where the labels m_n and $\bar{m}_n$ for individual neutrinos and antineutrinos are chosen to avoid double occupancy of any specific single-particle state. The average energy of individual neutrinos is on the order of 2–10 MeV. The density outside the neutrino-sphere is too small to reach even a quasidegenerate regime (see also Ref. [52]). For this reason, they can be regarded as essentially distinguishable (or Boltzmann) particles.

From the definitions in Eqs. (3) and (4) we see that each particle can be in a linear combination of N_f flavor states and a specific momentum mode. This implies that the many-body states $|\phi_n\rangle$ introduced above have a well-defined momentum and are eigenstates of the flavor-independent kinetic term H_0 in the Hamiltonian. One-body terms in the Hamiltonian H can be expressed more explicitly as

$$H_{1,v} = \sum_{i=1}^{N} H^v_{1,i} \qquad H_{1,m} = \sum_{i=1}^{N} H^m_{1,i}. \tag{7}$$

The first term describes vacuum oscillations and $H^v_{1,i}$ is the standard vacuum Hamiltonian containing the experimentally constrained mixing angles and mass squared differences,

$$H^v_{1,i} = U_f \begin{pmatrix} \frac{m_1^2}{2|\mathbf{k}_i|} & 0 & 0 \\ 0 & \frac{m_2^2}{2|\mathbf{k}_i|} & 0 \\ 0 & 0 & \frac{m_3^2}{2|\mathbf{k}_i|} \end{pmatrix} U_f^\dagger, \tag{8}$$

where U_f is the basis transformation from flavor to mass (for three flavors, it is the Pontecorvo-Maki-Nakagawa-Sakata matrix [53,54]) and m_j^2 are the squared masses of the energy eigenstates.

The neutrino matter coupling is described by the standard diagonal one-body potential arising from forward scattering from matter (assuming zero density of τ leptons)

$$H^{m}_{1,i} = \pm\sqrt{2}G_F(\Pi_e\rho_e + \Pi_\mu\rho_\mu), \tag{9}$$

where Π_x are projections on x flavor states, ρ_e ($\rho_{\bar{e}}$) and ρ_μ ($\rho_{\bar{\mu}}$) are the respective electron (positron) and muon (antimuon) densities, while G_F is Fermi's constant. The overall sign $\pm$ is for neutrinos and antineutrinos, respectively.

In astrophysical environments like core-collapse supernovae, the flux of neutrinos and antineutrinos is so large that the neutrino-neutrino coupling becomes significant [3,4]. The forward scattering neutrino-neutrino interaction between many-body states with fixed momenta for each neutrino takes the following form:

$$H^{fs}_{2,\nu\nu}(\{\mathbf{k}_i\}) = \frac{\sqrt{2}G_F\rho_\nu}{2N_\nu}\sum_{i<j}(1-\hat{\mathbf{k}}_i\cdot\hat{\mathbf{k}}_j)\vec{\lambda}_i\cdot\vec{\lambda}_j, \tag{10}$$

where the N_f component vectors of operators $\vec{\lambda}_i$ are the Pauli ($N_f = 2$) or Gell-Mann ($N_f = 3$) matrices acting on the different flavor amplitudes of each neutrino. The neutrino density is $\rho_\nu = N_\nu/V$, so the interaction can be written as independent of neutrino number for a fixed volume. An equivalent but more convenient parametrization of this interaction relies on the observation that

$$\vec{\lambda}_i\cdot\vec{\lambda}_j = 2P_{ij} - \frac{2}{N_f}, \tag{11}$$

where the P_{ij} is a flavor permutation operator exchanging each amplitude of one spinor with the other. Since the constant term does not affect time evolution, we can write for any N_f the forward scattering interaction as

$$H^{fs}_{2,\nu\nu}(\{\mathbf{k}_i\}) = \frac{\sqrt{2}G_F\rho_\nu}{N_\nu}\sum_{i<j}(1-\hat{\mathbf{k}}_i\cdot\hat{\mathbf{k}}_j)P_{ij}. \tag{12}$$

For the antineutrinos, the forward scattering contribution has a similar structure,

$$H^{fs}_{2,\bar{\nu}\bar{\nu}}(\{\mathbf{k}_i\}) = \frac{\sqrt{2}G_F\rho_{\bar{\nu}}}{N_{\bar{\nu}}}\sum_{i<j}^{N_{\bar{\nu}}}(1-\hat{\mathbf{k}}_i\cdot\hat{\mathbf{k}}_j)P_{ij}, \tag{13}$$

while for the mixed neutrino-antineutrino term, we have

$$H^{fs}_{2,\nu\bar{\nu}}(\{\mathbf{k}_i\}) = \frac{\sqrt{2}G_F\rho_{\bar{\nu}}}{N_{\bar{\nu}}}\sum_{i=1}^{N_\nu}\sum_{j=1}^{N_{\bar{\nu}}}(1-\hat{\mathbf{k}}_i\cdot\hat{\mathbf{k}}_j)Q_{ij}, \tag{14}$$

where we used $\rho_\nu/N_\nu = \rho_{\bar{\nu}}/N_{\bar{\nu}} = 1/V$. The operators Q_{ij} act on the flavor spaces of particles i and j as

$$Q_{ij} = \sum_{f\neq f'}|f,\bar{f}\rangle\langle f',\overline{f'}|. \tag{15}$$

The total energy is proportional to the number of neutrinos or the volume at fixed density, the same as the one-body terms. The neutrino-neutrino two-body interactions are representation independent for any orthonormal single-particle basis. It is the same in either the vacuum basis or the matter basis. The same is true for the neutrino-antineutrino interaction when the matter potential is either zero or large and the flavor basis is essentially the same as the matter basis. The general case is discussed later in Sec. VI.

Finally, the full interaction term including momentum exchanges can be written as

$$H^{fs}_{2,\nu\nu}(\{\mathbf{k}_i\}) = \frac{\sqrt{2}G_F\rho_\nu}{N_\nu}\int d^3\mathbf{q}\sum_{i<j}O_{ij}(\mathbf{q}), \tag{16}$$

where the operator $O_{ij}(\mathbf{q})$ acts on both the flavor and momentum space of particles i and j as

$$O_{ij}(\mathbf{q}) = h(\mathbf{q},\mathbf{k}_i,\mathbf{k}_j)\frac{1+P_{ij}}{2}|\mathbf{k}_i+\mathbf{q},\mathbf{k}_j-\mathbf{q}\rangle\langle\mathbf{k}_i,\mathbf{k}_j|, \tag{17}$$

while we introduce, following Ref. [38], the function

$$h(\mathbf{q},\mathbf{k}_i,\mathbf{k}_j) = f^*(\mathbf{k}_i+\mathbf{q},\mathbf{k}_j-\mathbf{q})f(\mathbf{k}_i,\mathbf{k}_j), \tag{18}$$

where we have defined (see [38])

$$f(\mathbf{p},\mathbf{q}) = \sqrt{2}\left(e^{-i\phi_\mathbf{p}}\sin\left(\frac{\theta_\mathbf{p}}{2}\right)\cos\left(\frac{\theta_\mathbf{q}}{2}\right) - e^{-i\phi_\mathbf{q}}\sin\left(\frac{\theta_\mathbf{q}}{2}\right)\cos\left(\frac{\theta_\mathbf{p}}{2}\right)\right). \tag{19}$$

Inclusion of the nonforward scattering is important because in an incoherent sum over paths the coupling between neutrinos' flavor in essence changes with time.

A. Time evolution and energy scales

To create a semiclassical approach to the time evolution it is useful to compare the energy scales of the various terms in the Hamiltonian. These scales control oscillation lengths and potential interference in the path integral describing time evolution.

The largest scale by far is the kinetic term H_0 since, as mentioned above, astrophysical neutrinos in these settings have energies of order 2–10 MeV. The associated oscillation lengths are $\hbar c/E$ or 20–100 Fermi. These oscillation lengths are of order 10^{-10} or smaller than the other oscillation lengths. This has important consequences and, as we discuss further below, suggests that a semiclassical treatment might be appropriate.

On the other end of the scale we have the vacuum oscillation energies. These are of order $\delta m^2/E \approx 10^{-4}$ eV^2/10 MeV or 10^{-11} eV. These scales are of order 10 km for δm^2_{23} and a 10 MeV neutrino, or even larger for the $\delta m^2_{12}/E$ mass scale. A substantial background matter

component can, however, dramatically shorten these oscillation lengths. For example, at electron densities of order $10^{38}/\mathrm{cm}^3$, the oscillation length for the electron flavor is of order one meter. This can be comparable to the scale of the neutrino-neutrino interaction in dense astrophysical environments.

In the region where neutrinos are dense but outside the protoneutron star core in a supernova, the two-body interactions have typical length scales ranging from centimeters to meters. In Ref. [52] we give an estimate of 1 cm at a radius of 50 km. At larger distances from the core, the density decreases like $1/R^2$, with an additional reduction from the more-forward scattering of up to another $1/R^2$. Nonforward scattering might slow the decrease of the interaction with distance to some degree. Forward scattering would give a length of approximately 1 m at a radius of 150 km, still dramatically longer than the H_0 scale but much smaller than the scale of the vacuum term. At 500 km, the distance would be roughly 100 m, still short compared to vacuum oscillation lengths, but perhaps comparable to vacuum plus matter.

III. TIME EVOLUTION AND KINETIC DECOHERENCE

The time evolution of the full system is governed by

$$|\Psi(t)\rangle = \exp[-iHt]|\Psi(0)\rangle, \tag{20}$$

where $|\Psi(0)\rangle$ is the initial state which we assume to be a single product-state of the form in Eq. (6) above. A more general incoherent sum of product states can be treated equivalently.

The time evolution is unitary, conserving the norm of the state. For this Hamiltonian the total numbers of neutrinos and antineutrinos are separately conserved. These can change from other processes like capture and emission that are not considered here. We do expect however that these processes will only enhance the decoherence.

The time evolution of the system can be written as a path integral with one- and two-body interaction terms. Since the one-body term can be solved explicitly, we rewrite it in a form where the one-body terms are explicitly included and insert two-body vertices at arbitrary times

$$\begin{aligned} e^{-iHt} = &\sum_{n=0}^{\infty}(-i)^n \\ &\times \mathcal{T}\int dt_n \int dt_{n-1}\ldots \int dt_1 \int dt_0 \sum_{i_n,j_n,\ldots,i_1,j_1} \\ &\times \exp[-iH_{01}t_n]H_{2;i_n,j_n}\exp[-iH_{01}t_{n-1}]\ldots \\ &\times \exp[-iH_{01}t_1]H_{2;i_1,j_1}\exp[-iH_{01}t_0], \end{aligned} \tag{21}$$

with the requirement that the total time $t = \sum_i t_i$. In this expression we have used $H_{01} = H_0 + H_{1,v} + H_{1,m}$, the sum of the kinetic, vacuum, and mass one-body terms, while H_2 is the sum of the neutrino-neutrino, antineutrino-antineutrino, and neutrino-antineutrino terms. Our approach then relies on sampling both the sum and the integral in the same spirit of stochastic series expansion versions of the quantum Monte Carlo method [55,56].

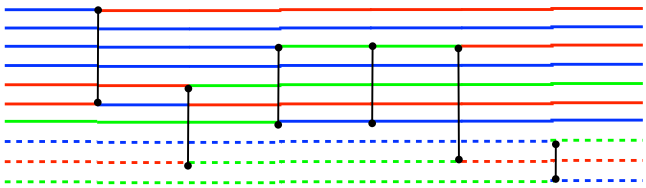


FIG. 1. Pictorial representation of the propagation represented by Eq. (21). Horizontal lines are neutrinos, dashed lines are antineutrinos, and color represents flavor. Vertical lines represent two-neutrino vertices. Only flavor evolution is indicated here, though the momenta are also changing at each vertex.

The one-body evolution through H_{01} is simple: an initial product state of neutrinos retains that character with phases from the vacuum plus matter Hamiltonian H_{01}. For convenience we use a local mass basis for the one-body evolution. A Trotter-like evolution where the one-body term is diagonal between each two-neutrino vertex is appropriate. If the neutrino flux is very low, as in the Sun, one has to include an explicit time dependence to account for the spatially varying matter potential. In this way the standard MSW limit is recovered in the limit of low neutrino density. Following the discussion in Sec. II A, in a supernova the timescale of two-neutrino interactions is shorter than that due to the changes in the mass density and we then take the $H_{1,m}$ Hamiltonian independent of time.

The two-neutrino interaction involves flavor and momentum amplitudes of two neutrinos at a time. In this equation we write $H_2 = \sum_{i<j} H_{2,ij}$ and sum over (or sample) individual pair operators in the path integral. Pictorially this can be described as shown in Fig. 1.

In this figure, different mass eigenstates or flavors are represented by the colors. The horizontal lines represent diagonal time evolution in the instantaneous mass basis between two-nucleon vertices. The vertical lines represent two-neutrino or neutrino-antineutrino interactions, which may change the flavors. The momentum directions can change at each vertex, but these changes are not indicated in the figure. The magnitude of the momenta can also change.

In two-neutrino scattering, the final states must conserve energy and momentum. Momentum is conserved by construction for an interaction that is a function of 3-momentum transfer. Energy conservation introduces a delta function in final- minus initial-state energy, reducing the dimensions of possible momentum transfer $\mathbf{q}$ to 2, as shown in Ref. [38] in the center of mass frame. Figure 2 shows possible final states in the lab frame for a specific set of initial momenta, projected into components parallel and perpendicular to the total momentum of the pair. There is

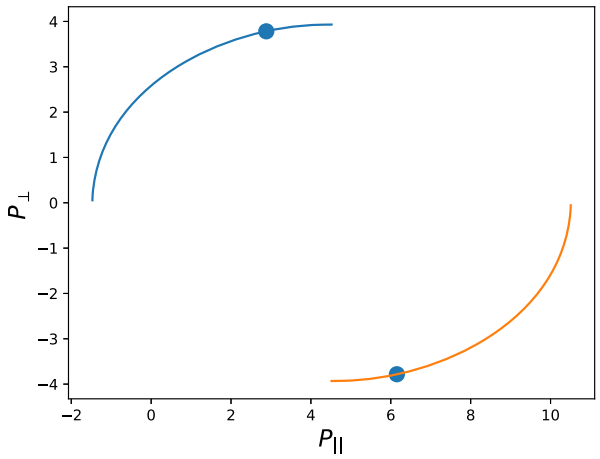


FIG. 2. Possible two-neutrino final states conserving momentum and energy. Sample initial states' momenta parallel and perpendicular to the total pair momentum are shown as circles. Possible two-neutrino final states conserving energy and momentum are shown as lines. The two final-state neutrinos each lie on one of the two lines. There is an additional azimuthal symmetry as well.

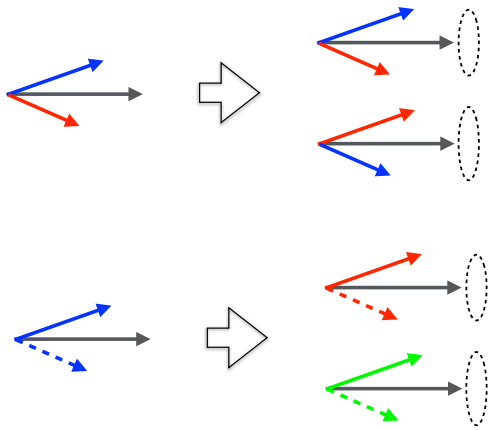


FIG. 3. Possible initial and final states in neutrino-neutrino (upper) and neutrino-antineutrino (lower) vertices, indicating azimuthal rotations and possible flavor changes. The sum of the two momenta and the individual magnitudes (kinetic energy) are conserved. The final states can either exchange the flavors in the upper panel or not. In the lower panel the momenta magnitudes can change (or not) between neutrino and antineutrino and the flavor of the pair can change. The dashed ovals are meant to indicate the possible azimuthal rotation of momenta in the final state, still preserving the total momenta.

also an azimuthal rotation possible for each pair and different possible flavor states, see Fig. 3. The flavors can change—a neutrino entering with a specific flavor and momentum can change either momentum or flavor, or both. The result is a two-dimensional surface of final-state momenta that conserve both energy and momenta with potentially more than one flavor state for each set of momenta.

The energy in the flavor degrees of freedom is very small compared to H_0, and in two-neutrino scattering, its energy can vary freely, with only the total energy being conserved through tiny variations in the magnitude of the momenta. The time-varying couplings from the scattering allow the flavor component of the energy to vary freely over the full many-body range.

It is valuable to compare full many-body evolution to a classical treatment where energy is exactly conserved at each scattering. One step beyond the classical treatment is to consider the evolution of a system including one initial particle in a bath of background neutrinos that are already equilibrated. This evolution is essentially what happens when a new neutrino is created in a background of N neutrinos, perhaps at high energy. The time evolution of this additional neutrino can be treated in linear response because one scattering of the "impurity" is incoherent from the next one. This happens because there are many more pairs of background neutrinos interacting at all times, and only one impurity neutrino. An example of this type of physics is an impurity ion created in an electron plasma in thermal equilibrium [57]. This goes beyond a classical treatment in that it includes virtual excitations of the new neutrino with all neutrinos in the bath, including possible momentum and energy exchanges. The total energy is conserved, but the division between an impurity and the background changes with time. Linear response treats the interaction of the background neutrinos to all orders but considers only one scattering of the new neutrino with the many-body system. As long as successive interactions of the original neutrino are incoherent, linear response should be sufficient. The evolution of this impurity neutrino is governed by $\int d\mathbf{q} \int d\omega \omega S(q,\omega)$, with limits of integration determined by the initial momentum and energy of the "impurity." The average time required for one scattering is determined by t times the sum of the magnitudes of all transition matrix elements from the initial state and is hence proportional to $1/G_F$. In a single scattering, the impurity will on average lose half of its energy since it can exchange with another neutrino. A few such scatterings will be sufficient to reach equilibrium. Detailed kinematics and their impact should be studied in more detail.

In the full many-body quantum evolution, virtual excitations are also crucial. Only after the full propagation over a time t, where all pair interactions are included, is energy conservation imposed. This gives potentially even more freedom than evolution with one impurity. The full evolution involves the time evolution of all particles simultaneously, so we expect a similar amount of time to be required. As in standard evolution with sufficient random coupling, the equilibration time will be governed by the variance: the expectation value of $\langle H^2 \rangle$ minus the expectation value of $\langle H \rangle$ squared. In a product state of spins, timed with plane waves in space, only the sum over spin terms for each pair contributes to the variance. The

resulting equilibration time t is of the order of the inverse of the variance per particle [58–60],

$$t \approx \pi/\sqrt{\langle (H_2/N)^2\rangle - \langle H_2/N\rangle^2}, \tag{22}$$

again proportional to G_F. The factors of 1/N are for extensive observables, the minimum average time for any exchange in the system is a factor of N faster. For an initial product state and a time-independent Hamiltonian the variance is $O(N)$ which implies this equilibration time is $O(\sqrt{N})$ (see also [52,61]). Note that this is a lower limit on the equilibration time resulting from assuming no interference.

In addition we can estimate the increase in equilibration time from enforcing energy conservation in the kinetic term at each vertex. The result is a two-dimensional surface at each vertex, as for the two-body case. This only increases the equilibration time by a modest factor of 3–4, obtained by estimating the ratio of states without energy conservation as compared to with energy conservation at each vertex, and then equating the number of states reached in the two cases for different finite times [see Eq. (A5)]. This insensitivity is due to the exponential growth of the number of nonzero amplitudes with time, as discussed below.

The difference from the forward-scatting case is that the implicit spin Hamiltonian here is time dependent so what matters is the average variance over time. We can get a constant timescale if the variance becomes proportional to N^2 on a timescale that does not depend on N, as is expected for an auxiliary field treatment of short-range interactions. The variance is basically given by the sum over all pairs and all momentum transfers from the initial state to all one-pair momentum transfers. The variance here is somewhat larger than for forward scattering calculations, hence the timescale is similar or shorter. For forward scattering only terms that exchange spins enter the variance. Those same terms enter here along with contributions from terms diagonal in the spin but off-diagonal in momenta. The spin exchange terms are the same in the two calculations, but in the full angular-dependent coupling the amplitudes are spread over many incoherent momentum modes. This timescale is considerably shorter than the standard distance scale of the inverse of the two-body cross section times the density obtained in purely classical calculations, as we show in more detail in Appendix A. The rapid equilibration depends upon the short-range nature of the interaction and could be tested in cold atom experiments [62]. In such experiments the two-body interaction can be rapidly increased from essentially noninteracting to a finite scattering length, and we expect equilibration times for low to modest interactions to scale with the inverse of the scattering length.

The dephasing effect caused by the large kinetic energy scale is often called "kinetic decoherence." As it arises from the flavor-independent kinetic terms, it essentially implies that different paths with different momenta for the neutrinos do not interfere. The spatial part (momentum directions and amplitudes for each neutrino) can essentially be treated classically, however, in a full calculation, energy conservation must be considered for the initial and final states. In the quantum time evolution, this yields a random overall phase for each neutrino as a function of time, with a constraint only on their sum. Enforcing energy conservation at each vertex implies only a single overall phase for all the momentum degrees of freedom, which does not impact observables.

In principle, for the same kinematic (momentum) paths, the relative phases of different neutrinos could still interfere. The flavor state of the system is essentially described by permutations of the original flavors plus conversions of neutrino-antineutrino pairs of one flavor to another. Since it is an all-to-all interaction, one pair exchange is rapidly followed by another between a different pair, leading to an entangled many-body state which, however, locally (i.e., for individual neutrinos) will look indistinguishable from an incoherent flavor state. In the interior, where the eigenstates are split by larger effective δm^2, this also contributes to flavor decoherence.

Potential interference between different flavor amplitudes of individual neutrinos remains. This is the interference that gives rise to the MSW effect, and should remain in the limit of low neutrino density. Using the fact that different spatial paths do not interfere, we can make predictions about the time-dependent expectation values of single neutrino observables without keeping track of all the phases that would be required to reverse the unitary time evolution and return to the initial state. This is the essence of equilibration or thermalization in quantum evolution discussed in previous publications [52]. Here, the neutrinos equilibrate very rapidly, subject to symmetries including energy and momentum conservation, as well as conservation of the total number of neutrinos and the total number of antineutrinos.

IV. SEMICLASSICAL APPROXIMATIONS

To compute semiclassical approximations to one-body observables as a function of time, we take advantage of the rapid decoherence in two- or more-body neutrino amplitudes to write them as a sum over incoherent paths defined in the product space. The times between vertices are governed by the inverse of the sum of the magnitudes of the two-body off-diagonal matrix elements, and the sampling of specific off-diagonal transitions is taken from the scaled sum of the squares of various possible off-diagonal matrix elements. Since the different paths are nearly incoherent and each contributes a positive contribution to the probability, Monte Carlo methods can be used to sample the times and the transitions. This is represented for a single path in Fig. 4. The vertical bar represents the time where expectation values are taken.

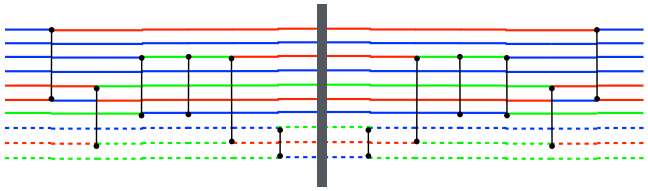


FIG. 4. Pictorial representation of the calculations of observables at the black vertical bar from the squares of the relevant amplitudes. The path integral on the left and right is the same with phase information remaining from flavor amplitudes within each neutrino.

For constant background densities of leptons, the one-body interaction is constant in time. In this case, we take the initial state to be a product state of neutrinos in the mass basis. In this basis, the $H_0 + H_1$ is diagonal and can be represented, up to a phase, by specific mass states invariant in time (represented by a single color connecting each two-neutrino vertex). The random exchanges of flavor and momenta give rise to equilibration of the energy of the different flavors of neutrinos. The rapid random conversion of $\nu\bar{\nu}$ pairs of a given flavor or mass state to another flavor or mass state gives rise to an equilibrium condition,

$$\rho(\nu_e)\rho(\bar{\nu}_e) = \rho(\nu_\mu)\rho(\bar{\nu}_\mu) = \rho(\nu_\tau)\rho(\bar{\nu}_\tau), \tag{23}$$

for a given initial difference between the numbers of neutrinos and the numbers of antineutrinos in each mass eigenstate,

$$\Delta_{\nu\bar{\nu}} = \rho_\nu - \rho_{\bar{\nu}}. \tag{24}$$

This difference remains fixed for Dirac neutrinos in a constant background matter density. The equilibration is simplest in mass eigenstates, but at large electron and muon densities, the flavor and mass eigenstates coincide, resulting in equilibration in both mass and flavor. This equilibrium will hold in any environment where the mass eigenstates of neutrinos and antineutrinos coincide. These results have been discussed extensively in [52].

With the semiclassical picture, we can also explore the time evolution in a spatially varying background matter density or for smaller finite constant background densities, where the mass eigenstates of neutrinos and antineutrinos do not coincide. Previously, the equilibrium distribution did not depend upon microscopic details other than the symmetries of the Hamiltonian. Here, the time or distance scale of the two-neutrino interactions versus variation in background density can play an important role.

To evaluate observables as illustrated in Fig. 4, we need to average over paths. Starting from a product state, one computes the nonzero matrix elements H_{ij} to all possible future states j. The Hamiltonian is a sum of pair terms, so for each pair, we can calculate the sum of the magnitudes of the off-diagonal matrix elements. The time for this vertex can be obtained by sampling from an exponential distribution with time proportional to the inverse of this sum. This represents the time to evolve into any orthogonal state. To evolve, one picks the shortest time from those obtained for all pairs.

The particular final state chosen is taken from the squares of the transition amplitudes, normalized to one for all transitions. In this manner, one is incorporating unitarity, the correct time dependence, and the probability of landing in a particular state. At this point, we have a new product state and can repeat the process. All the previous pair times from pairs not involving either of the chosen pair are retained, while those involving either of the chosen pair are resampled from the new off-diagonal matrix elements. This method retains independent evolution of clusters of neutrinos that do not interact.

For a concrete example, assume we start with an initial product state. For a given pair (i, j) at short times δt the transition probability can be approximated as

$$T_{ij}(\delta t) = \sum_{k\neq m_i, l\neq m_j} |\langle \psi_k, \psi_l | \delta t H_{2;ij} | \psi_{m_i}, \psi_{m_j}\rangle|, \tag{25}$$

where the sum is over possible orthogonal final states with momenta and flavors. This expression is valid for short times δt, for an isolated pair. The amplitude of each state orthogonal to the initial state grows linearly in time,

$$\alpha_j(\delta t) = V_{ij}(\delta t), \tag{26}$$

where i is the initial state and V_{ij} is the transition matrix element of the Hamiltonian. In our semiclassical algorithm, the extremely short-time behavior can be better approximated by taking the time as the larger of two times sampled from above, since the expectation value changes only when both the left- and right-hand sides of the propagation include a transition.

Note that we can change the time propagation to $\exp[-i(H - E_0)t]$ without changing the observables. Here we take E_0 to be the sum of the kinetic energies of the individual neutrinos. For energy-conserving time propagation we can split this into a sum of phases for each neutrino so mass eigenstates do not precess. Any state with the same total kinetic energy, arbitrarily divided into energies for each neutrino, can be treated this way.

At very short times the amplitude for off-diagonal transitions is linear in time and proportional to $G_F t$, so the probability of these new states is proportional to $(G_F t)^2$. The total transition probability for an out-of-equilibrium neutrino impinging on an eigenstate, thermal state, or any time-independent background state will then reduce to a sum of incoherent cross sections for each possible transition.

For larger times the number of orthogonal states with finite amplitudes grows exponentially in time assuming no

interference between paths. The spin-momentum basis for each neutrino is very large and interference is essentially absent. The amplitude of the initial state is governed by unitarity and its amplitude decays quickly and hence the one-body expectation values rapidly approach the equilibrium value.

We apply the algorithm to the given initial many-body product state. The interaction time for each pair can be sampled from $\exp(-\sum_j |V_{ij}|t)$, where the sum over j runs over all final states with a finite matrix element to the initial state i. After the interaction time is determined for each pair, the chosen two-neutrino vertex is determined by the shortest time. After this vertex we have to choose from all the various possible transitions for each pair. We can choose these from the normalized sum of the squares of all possible final states. In this manner a single product-state transitions to a single different product state.

Each orthogonal final state remains orthogonal during further time evolution due to the unitary nature of the time evolution. Therefore, the unitary evolution is preserved once we average over paths. We have the full path history of each individual flavor amplitude, allowing us to calculate any one-body observable as a function of time, in particular, any possible correlations between flavor and momentum or the number of neutrinos and antineutrinos of each flavor. This is all we need since, in the astrophysical neutrino problem, one can really only measure one-body observables and the correlations between them.

We can then perform the diagonal propagation for the next two-neutrino vertex and repeat the entire procedure until we reach the desired final time or distance. Note that in the next and subsequent steps, the interaction times of particles not in the chosen pair are retained. Those pairs involving one of the chosen pair are resampled from the current time plus the sample of the inverse magnitudes of the updated state. The end point will be a product state of mass basis neutrinos.

Of course, in general, there can be interference between paths, and if so, this semiclassical approximation will fail. The fact that the neutrinos are nondegenerate with large kinetic energies means that correlations between different neutrino flavors and momentum rapidly decohere, leaving only interference between the flavor amplitudes of each individual neutrino.

V. SEMICLASSICAL VERSUS FULL HAMILTONIAN SIMULATIONS

In Fig. 6, we compare the evolution of a small number of neutrinos (5 ν_e, 3 ν_μ, and 2 ν_τ) using $\exp[-iHt]$ for the full forward scattering Hamiltonian to the semiclassical approximation for 100 neutrinos in the same ratio of flavors and the same energy distribution for each flavor.

We do not include the momentum degrees of freedom in the full Hamiltonian simulation. The full quantum calculation is difficult with momentum because of the large number of states: three spin states times a very large number of momentum states for each neutrino. The semiclassical calculation can be carried out for hundreds of neutrinos at the same density. In this case we can also resample the directions of the neutrinos at each vertex, and here we sample the neutrino directions randomly from a hemisphere each time they are scattered.

We choose an initial condition so that the energy of the electron neutrinos varies uniformly from 4 to 6 MeV, while the mu and tau neutrinos vary uniformly from 9 to 11 MeV. The average initial electron neutrino energy is 5 MeV, while the ν_μ and ν_τ are 10 MeV. All neutrino directions are initialized randomly on a hemisphere.

For this initial calculation, we propagate for a total scaled time of 10 μ^{-1} with $\mu = \sqrt{2}G_F\rho_\nu$. The exchange matrix element is then

$$M_{ij} = \frac{G_F}{\sqrt{2}} \frac{\langle \lambda_i \cdot \lambda_j \rangle}{N} (1 - \hat{\mathbf{k}}_i \cdot \hat{\mathbf{k}}_j). \tag{27}$$

The time between nondiagonal interactions for an individual pair is distributed as

$$P_{ij}(t) \propto \exp\left(-\sum_{j \neq i} |M_{ij}| t \right) \tag{28}$$

and is proportional to $1/N$ from the matrix element. The next time for any transition involving particle i is then independent of N because there are N-1 pairs for each neutrino.

The shortest time among all pairs is used as the next interaction time. This time is proportional to $1/N$ since there are N particles to choose from. Therefore even the semiclassical calculation is slightly more difficult for larger N. We can easily propagate of order 100 neutrinos on a laptop in this way.

In the limit of zero interference between different paths, the equilibration time for one-body observables is independent of N (see Appendix B). This result depends on having a vertex that changes both flavor (spin) and momenta for a pair. We have compared semiclassical calculations of 100 neutrinos to verify this conclusion. The semiclassical results are identical within statistics for 10 neutrinos or 100 neutrinos at the same density. The algorithm will retain this independence for arbitrarily large N with a computational cost proportional to N^2.

Note that the energy in the flavor (spin) correlations is not conserved on its own, but only when combined with the one-body Hamiltonian. The energies in spins are of the order of 10^{-10} that of H_0, so small variations can easily be absorbed into tiny fluctuations of the neutrino momenta. This is a significant difference from traditional mean-field calculations on fixed grids particularly in 1D. It is similar to fixed random couplings, but the evolution to the equilibrium state is faster.

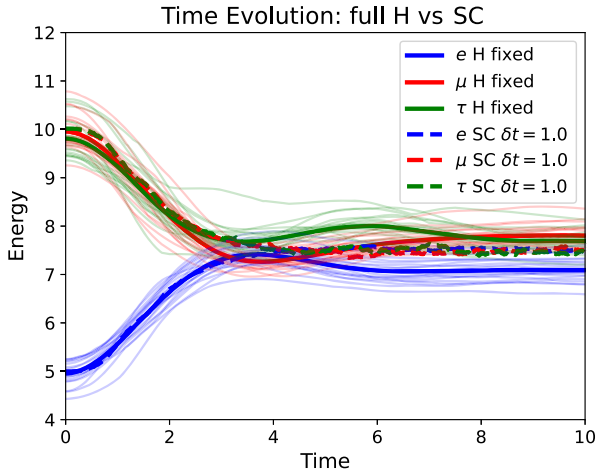


FIG. 5. Full semiclassical calculation for large N versus explicit many-body calculations of 10 neutrinos. Average of 10 many-body calculations are indicated by thick solid lines, with individual runs by fainter runs. Thick dashed lines are obtained by averages over many semiclassical runs with different samples of energies and momenta for 100 neutrinos. The full H calculation is an average over instances of fixed couplings, while the semiclassical runs resample the couplings at a rate of 1 μ^{-1}.

The sampling procedure here does not necessarily conserve the magnitude of the total energy dominated by the neutrinos' kinetic energy, unless one arbitrarily enforces energy conservation, either at each vertex, after some number of insertions, or more globally. In the path integral expression for time evolution, energy conservation is only enforced after the end of the time evolution. This is only a one-dimensional constraint on the final momenta of all N neutrinos, though. In principle one could worry that this constraint would impact the equilibration timescale. In Refs. [38,51], they enforced exact energy conservation at each vertex in a lattice simulation and did not find a large impact. This constraint would be more restrictive in a continuum treatment of the neutrinos, as the final states are restricted to a two-dimensional subspace of the three-dimensional $\mathbf{q}$. However, the true path integral requires energy conservation only at the end of the time evolution. Paths where one pair gains energy at the expense and another loses the same energy and further generalizations are allowed. There are $\mathrm{N}(\mathrm{N}-1)/2$ pairs each with a momentum transfer q in the Hamiltonian, so one three-dimensional constraint will allow a huge number of momenta transfer for the various pairs. After $N(N-1)/2$ pairs essentially any final state can be reached. In classical physics, the equilibration timescale is $1/\rho_\nu \sigma_{\nu\nu} c$, where $\sigma_{\nu,\nu}$ results from energy conservation at each vertex (see Appendix A), and is much longer than the true equilibration time, as it is proportional to G_F^{-2}.

In Fig. 5 we compare the semiclassical calculations to full many-body quantum simulations with random couplings on a hemisphere. We use only 10 neutrinos for the full calculations, as each can be in one of three flavor states, yielding a large number of total amplitudes. The initial couplings are chosen from a uniform neutrino direction on the hemisphere. These directions and the couplings are kept fixed in this calculation, since it is not possible to match a spin Hamiltonian to the full Hamiltonian exactly. The semiclassical method can randomly resample couplings at each interaction vertex. For $N = 10$, the oscillations at larger times are due to the small number of neutrinos, and are at a very small scale compared to the original energy differences. The thick solid lines are obtained as an average over 10 full Hamiltonian calculations with different samples for the initial condition. The faint lines indicate individual many-body calculations.

The thick dashed lines are averages over 100 semiclassical calculations with 100 neutrinos each. In these calculations we sample the first $N/2$ time steps from each run from the greater of two samples of the magnitude of the matrix element, which results in a quadratic behavior near $T = 0$. The initial alignment of flavor states requires both left- and right-hand paths in the path integral to flip to change the expectation value, thus, picking the larger of two times for the chosen pair gives the correct quadratic behavior in time for the correlation function. After the first $\sim N/2$ exchanges, the spins are no longer in flavor eigenstates, therefore, we just sample from a single exponential. To gauge the effect of the varying couplings, the updated directions of the momenta are chosen randomly from the hemisphere (the same sampling as for the initial configuration).

The semiclassical calculations give the correct equilibrium distribution, the correct timescale for the equilibration, and can easily accommodate hundreds up to one thousand neutrinos. These results should be contrasted with previous full many-body calculations performed considering only two neutrino flavors and only the forward scattering interaction: these lead to typical evolution timescales growing with system size depending on the initial condition and the geometry of the system [23,24,26,28].

The equilibration time for one-body observables can be different than complete equilibration. In addition, different timescales for the two-body interactions and the change of coupling may give different scaling results. For the spin-only Hamiltonian, very slow changes will lead to the growth of many-body equilibration time with N since the energy variance of the initial product state is proportional to $\sqrt{N}$ for our Hamiltonian, where the total spectral width is proportional to N. General equilibration cannot be faster than the inverse of this variance.

A slow change in the spin Hamiltonian will essentially reproduce fixed Hamiltonian results. Very rapid changes will give a diffusion of the spin coordinates, again slowing equilibration. In the physical system considered here, the coupling changes at each vertex. Some two-neutrino vertices do not change flavor, but they are comparable

to or smaller than those that change both momentum and flavor, resulting in changes in coupling on timescales comparable to the spin term. Extremely fast changes will induce a diffusionlike scaling for equilibration.

We find that one-body observables at constant density equilibrate within a constant time as a function of N for the full Hamiltonian with its implicit time dependence. For a time-varying Hamiltonian, the full many-body equilibration time is expected to be logarithmic in N, while for fixed Hamiltonians it should increase as a power of N. The randomness reduces the size dependence of the one-body equilibration.

There is a strong similarity between this problem and the problem of random quantum circuits, much discussed in condensed matter [63]. These circuits are often very fast scramblers [64], particularly for the one-body observables we consider here. In our case, there are important symmetries that need to be included (conservation of neutrino and antineutrino number, number of neutrinos minus antineutrinos of each flavor, etc.). The very rapid equilibration arises because the neutrinos are nondegenerate, hence, there is no Pauli blocking. The short-range interaction allows coupling to many possible transitions at each time, and the kinetic energy of the neutrino momentum dominates energy conservation, enabling large fluctuations in the flavor energy.

As shown in Ref. [52], the neutrino-antineutrino interactions also lead to rapid equilibration in the neutrino and antineutrino densities of each flavor. As we discuss below, this equilibration is easiest to see with very large matter background densities or for nearly vacuum conditions. In these cases, the flavor eigenstates of the neutrinos and antineutrinos are identical. Below, we consider modest constant background densities and varying densities governed by MSW evolution, where the background matter density is changing.

VI. MODEST MATTER DENSITIES

Unlike the vacuum case or the case of large matter densities, at more modest densities, the mass eigenstates of neutrinos and antineutrinos are not identical. In such a case, we cannot rotate the Hamiltonian to a basis where the neutrino-antineutrino interaction simply changes the flavor of the final pair relative to the initial pair. One can only rotate to either the neutrino mass eigenstates for both neutrinos and antineutrinos, or to the antineutrino mass eigenstates for both.

It is simplest to consider rotating both to the majority eigenstates, either neutrinos for the $N_\nu > N_{\bar{\nu}}$ or antineutrino mass eigenstates for $N_\nu < N_{\bar{\nu}}$ instead. The neutrino-antineutrino interaction will then cause a very rapid equilibration in this basis, but the minority species is not in a one-body mass basis and will slowly evolve. It may be that the background densities are evolving more rapidly than this, and hence one should consider the MSW case with spatially varying densities.

Full equilibration will occur on scales associated with the mass differences squared of the minority species. If only one background density is large and only one mass state is identical for neutrinos and antineutrinos, it should be possible to define an equilibrium between the product of densities of this flavor and the sum of the products of the other flavors, where the neutrino and antineutrino states do not coincide.

A. MSW conversions including neutrino-neutrino interactions

The results of Ref. [52] demonstrate the rapid equilibration of momenta (magnitude and angles) of different flavors of neutrinos and antineutrinos in the presence of a sizable background matter potential or in the vacuum. The MSW matter potential yields neutrino eigenstates that correspond to flavor eigenstates for electron neutrinos and antineutrinos and for all flavors if there is a significant net muon contribution to the background. It is important to understand what happens as the matter background decreases at larger distances.

MSW resonances typically occur at radii of 10^3 to 10^5 km in core-collapse supernovae [65]. The importance of neutrino-neutrino couplings for this wide range of distances can vary significantly. Standard arguments based upon forward scattering imply a $1/R^4$ scaling of the two-body terms relative to the single neutrino terms. The 1 cm length scale at 50 km above translates to 1.6 km at 1000 km or 1.6×10^5 km at 10^5 km. With nonforward scattering, though, the average angular dependence could be nearly constant giving a $1/R^2$ scaling and an equilibration length of 4 m at 1000 km or 40 km at 10^5 km. The impact will vary greatly with the time-dependent luminosity, but the neutrino-neutrino interaction can potentially play a role even in MSW regions. We consider two different regimes where the two-neutrino interaction could play a role: (1) a very rapid variation in density scale relative to the two-body interaction scale and (2) the adiabatic case where the two-body interaction scale is short compared to the density variation scale.

We first consider the simplest case of neutrinos only going through an MSW resonance. Without neutrino-neutrino interactions, the standard MSW evolution occurs, with potential dependence on the neutrino energy, as the resonance occurs at slightly different densities for different energies. With neutrino-neutrino interactions, one can track the evolution of each flavor of neutrino, with momenta being exchanged through the two-neutrino interactions. The evolution of each initial energy neutrino then becomes independent of energy, and the neutrino evolution for each neutrino is equal to the standard MSW evolution with an inverse energy equal to the average energy of the neutrinos. Note that the exchanges conserve this average energy over

all neutrinos. We have verified this result with explicit semiclassical calculations.

We assume a specific initial condition where the electron neutrinos dominate as expected, for example, during the neutronization burst (see [66] and references therein). Without oscillations, the energies of the electron neutrinos are expected to be, on average, lower than those of the other flavors, as they decouple later. However, the neutrino interactions rapidly equilibrate the neutrino and antineutrino momenta. We take as an example a state that is already equilibrated by passing through a high-density region. We take neutrinos and antineutrinos in initial conditions with flux ratios given by $9:1:3:3:3:3$ for $\nu_e:\bar{\nu}_e:\nu_\mu:\bar{\nu}_\mu:\nu_\tau:\bar{\nu}_\tau$. We consider two limiting cases for the evolution of the matter density: a rapid quench in the matter potential and a slow adiabatic reduction of the background density. These two limiting cases provide a picture of what will happen in general.

The rapid quench case is simple in that we can consider the instantaneous overlap of the mass eigenstates before and after the quench. Here we take a quench to zero matter density, so we use vacuum eigenstates after the quench. The initial distributions will be governed by the equilibration described above: equal densities for the product of neutrino and antineutrino mass eigenstates (at high densities, also flavor eigenstates) and equal energy distributions. For an instantaneous quench, we can simply calculate the instantaneous transition to the vacuum eigenstates. These new distributions in terms of the vacuum eigenstates will then rapidly equilibrate through the change of flavors (mass eigenstates) of neutrino/antineutrino pairs.

The quench result for the initial conditions described above is shown in Fig. 6. The initial densities are on the left, corresponding to vacuum densities shown in the middle, and final equilibrated densities on the right. The difference

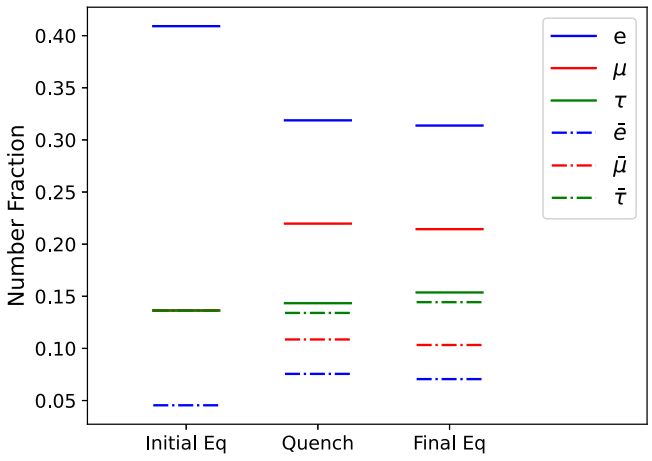


FIG. 6. Dynamics for the rapid quench of the matter density. The initial distribution is shown on the left, this corresponds to the vacuum flavor distribution shown in the middle, which equilibrates to the relative densities shown on the right.

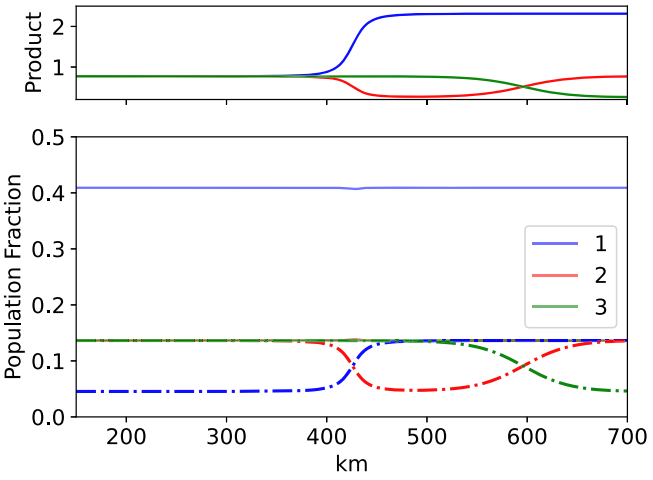


FIG. 7. Standard MSW in the neutrino mass basis for both neutrinos and antineutrinos. Neutrinos are shown as solid lines, antineutrinos as dash-dot lines. The neutrino evolution is nearly adiabatic (constant), and the antineutrino density is nearly adiabatic in the antineutrino basis, but evolves with time in the neutrino mass basis, breaking the flavor equilibration arising from neutrino-antineutrino interactions.

between electron neutrino and antineutrino densities becomes smaller, while the others are largely unchanged. This is due to the initial and final overlaps of the mass eigenstates at high density and zero density. For these calculations, we assume a normal mass hierarchy.

At the other extreme, we consider slow evolution of the matter densities for the same initial conditions. Here we show results for an exponentially decaying profile of the form $\rho_e - \rho_{\bar{e}} = \rho_0 \exp[-(r/s)]$, starting at 150 km and with a scale height of 25 km, and neutrinos and antineutrinos equilibrating to an average energy of 5 MeV.

The standard MSW evolution in this nonstandard antineutrino basis is shown in Fig. 7. The lower panel shows neutrino (solid lines) and antineutrino densities (dashed lines) in the neutrino mass basis. Neutrino densities are nearly flat as the evolution is close to adiabatic. The antineutrino densities would also be nearly flat if plotted in the antineutrino mass basis. Here, though, we transform them to the neutrino mass basis to see how the initial equilibrated state evolves under MSW evolution alone. The upper panel shows the product of neutrinos and antineutrinos in the neutrino mass basis. This shows a significant deviation from equilibration once the neutrino and antineutrino mass eigenstates do not align, for this case around 300 km.

The initial state has a relatively large number of electron neutrinos and a small number of electron antineutrinos, represented by solid and dashed blue lines in the figure. For neutrinos, this is the highest mass state at high density. Since the initial number of electron antineutrinos is small, the corresponding density (blue dashed line) is also small. As expected in an adiabatic conversion, the highest mass

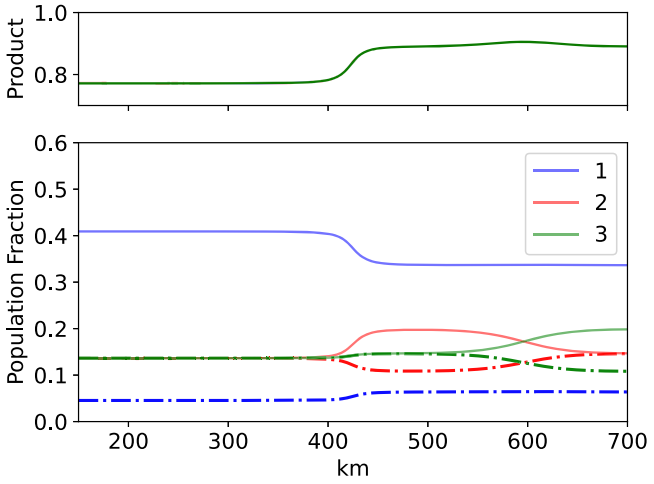


FIG. 8. Standard MSW plus flavor equilibration in the neutrino mass basis for both neutrinos and antineutrinos. Both neutrino and antineutrino densities evolve with time due to the flavor equilibration.

state remains the highest mass state as we evolve to the final vacuum Hamiltonian, and their flavor changes from electron to mu or tau. The mu and tau neutrinos are converted to all flavors. The antineutrinos do not undergo an MSW resonance in this case, however, the fact that the neutrino states do implies that the antineutrinos evolve when plotted in the neutrino mass basis. The antineutrino flavor densities are evolving, as the densities of antineutrinos in the neutrino mass basis are not constant. At large r, starting around 300 km, the deficit changes from electron flavor to μ flavor and then to τ flavor, corresponding to neutrino basis MSW resonances in electrons to the other flavors.

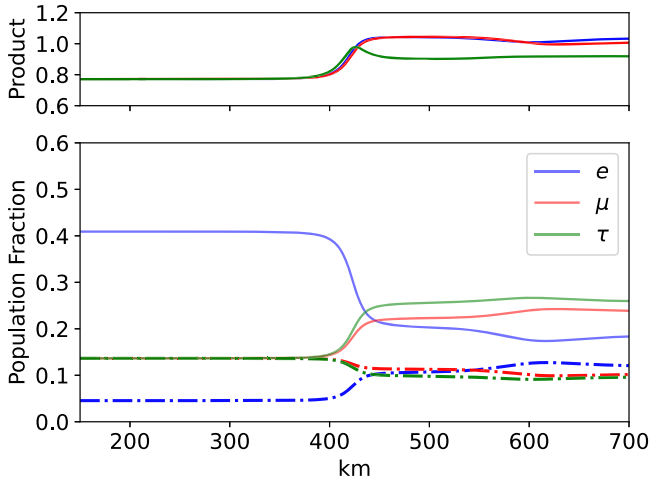


FIG. 9. Standard MSW plus equilibration in the flavor basis. The upper panel shows a slight remaining imbalance because we are equilibrating in the neutrino mass basis for the antineutrinos (fast equilibration) and not including the slower equilibration from pure flavor equilibration (see the text).

If the timescale of the neutrino-antineutrino coupling is very small compared to density variations in MSW, we can calculate its effect by equilibrating the product of densities in the instantaneous neutrino mass basis. The results of this equilibration are shown in the neutrino mass basis in Fig. 8. Since these densities are initially equilibrated, the rapid transitions of the ν_e density are offset to some degree by flux coming back from ν_μ, $\bar{\nu}_\mu$, and ν_τ, $\bar{\nu}_\tau$.

Transforming these results directly to the flavor basis for neutrinos and antineutrinos is shown in Fig. 9. The electron neutrino density is reduced, but not as much as in the MSW only calculation. A small difference in the product of flavor densities remains because we have only included the fast equilibration in the neutrino flavor basis, not the slower equilibration related to the single-particle antineutrino evolution in its own mass basis rather than the neutrino mass basis (see the text).

Finally, we compare the flavor densities for neutrinos and antineutrinos with MSW plus neutrino-antineutrino equilibration to the MSW evolution alone in Fig. 10. In the figure, solid lines represent neutrinos, while dashed lines represent antineutrinos. MSW only results are shown as thin lines, while MSW plus equilibration are represented as thicker lines. The flavor transition probabilities of the majority (electron neutrinos) are reduced by flavor equilibration. The MSW evolution reduces the electron neutrino density, but this reduction is partially compensated by neutrino-antineutrino interactions. The minority antineutrinos change fractionally more than the neutrinos since each vertex converts one pair to another flavor or mass state. In the limit of large ratios of neutrinos to antineutrinos, the evolution of the majority (neutrinos or antineutrinos) reduces to the standard MSW result.

The final results are closer to full equilibration among all flavors than MSW alone, but the impact is reduced for large or small neutrino to antineutrino ratios. The main impact is to somewhat inhibit MSW conversions, and this impact

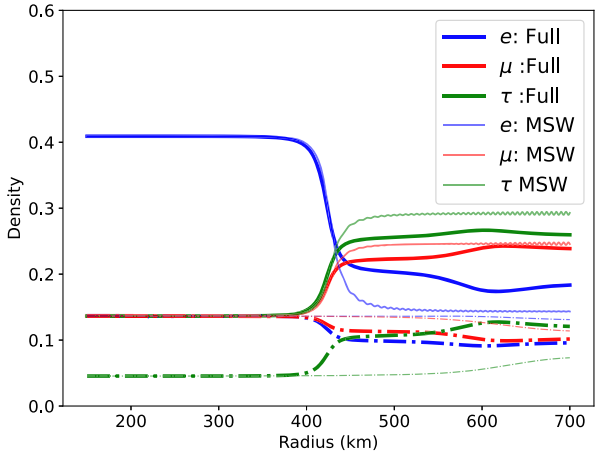


FIG. 10. Comparison of MSW plus neutrino-antineutrino evolution to MSW alone.

will be larger for more equal neutrino and antineutrino populations.

All the data used to produce the results shown in the figures are publicly available in Ref. [67].

VII. CONCLUSIONS

The essential features of neutrino evolution in astrophysical environments can be described in a semiclassical approach due to the fast decoherence timescales. These timescales would only be quicker by adding production or absorption processes due to their incoherent nature.

Decoherence leads to very fast equilibration between the energies of different flavors, essentially independent of the initial angular distributions of each flavor. In regions with high mass density, the number of neutrinos minus the number of antineutrinos in each mass eigenstate is conserved. The neutrino-antineutrino flavor-changing processes lead to an equilibration in the product of the neutrino and antineutrino densities of the different species. For this reason, a significant memory of the initial state will be retained, particularly when there is initially a large imbalance between the total numbers of neutrinos and antineutrinos.

The impact of this equilibration in neutron star mergers has been studied in Ref. [68]. They find that neutrino flavor transformations impact the composition and structure of the remnant, potentially leaving an imprint on the postmerger gravitational wave signal. They also have a significant impact on the composition and nucleosynthesis yields of the ejecta.

The neutronization burst in a supernova will produce many more electron neutrinos than antineutrinos. In contrast, in a neutron star merger, many neutrons are converted into protons, leading to a large production of electron antineutrinos. In each case, a strong memory of the initial conditions will be retained, and the energy of the electron neutrinos and antineutrinos will equilibrate with the other species, leading to a potentially significant effects on energy deposition in matter and nucleosynthesis.

Fast flavor instabilities in core-collapse supernovae have been studied in several works, including [69–71]. These have been performed incorporating mean-field approaches for the neutrino dynamics, which evolve quickly but are quite distinct from the evolution we obtain. In particular our results do not depend on crossing in angular distributions. Here energy equilibration of different flavor occurs quite rapidly everywhere. Our approach implies rapid local equilibration of the product of neutrino and antineutrino densities. Both of these differences could significantly impact energy deposition into the surrounding matter. It can also dramatically impact nucleosynthesis, because of the big impact of the energy and flavor-dependent charged and neutral currents. In principle it can also be studied with terrestrial neutrino detectors which can measure the time and energy flux of different neutrino flavors. Initial studies of this rapid equilibration in neutron star mergers have shown a significant impact [68].

This memory will be partially erased further out from the neutrino-sphere during adiabatic or near adiabatic MSW transitions, leading to a more constant ratio of neutrinos to antineutrinos in all flavors (see also [72]). In the case of core-collapse supernovae, this prediction could in principle be checked by terrestrial observations and/or nucleosynthesis observations.

This approach leads to many important topics not considered here, including the impact (if any) of Majorana neutrinos versus the Dirac neutrinos considered here. More studies on the impact of the hierarchy are warranted, as well as various types of initial conditions. A quantitative characterization of the equilibration timescale in regions with a large neutrino flux will also require further studies, particularly in assessing the role played by many-body correlations, which are directly responsible for neutrino thermalization. Finally, studies of the impact of neutrinos in the early Universe could be revisited.

ACKNOWLEDGMENTS

We thank Vincenzo Cirigliano and George Fuller for valuable conversations. This work was supported by the Quantum Science Center (QSC), a National Quantum Information Science Research Center of the U.S. Department of Energy (DOE), and by the U.S. Department of Energy, Office of Science, Office of Nuclear Physics (NP), Contract No. DE-AC52-06NA25396.

DATA AVAILABILITY

All the data generated to produce the figures present in the paper, together with a Jupyter notebook showing how to prepare the figures, are freely available through the Zenodo repository. A direct link to the repository is provided as Ref. [65] in the paper.

APPENDIX A: TWO-NEUTRINO PHASE SPACE AND ENERGY CONSERVATION

In this appendix, we describe the two-body phase space, including energy conservation for final states of two neutrinos with 3-momenta $\mathbf{p}_1$ and $\mathbf{p}_2$, conserving momenta and energy. We assume the matrix elements are short-range and thus independent of the magnitude of the vector 3-momentum transfer $\mathbf{q}$. The total momentum is $\mathbf{P} = \mathbf{p}_1 + \mathbf{p}_2$, and we can also calculate the magnitudes of the parallel and perpendicular components of each momentum relative to $\mathbf{P}/2$,

$$p_{||} = \mathbf{p}_i \cdot \hat{\mathbf{P}} - \mathbf{P}/2,$$
$$p_{\perp} = \mathbf{p}_i \times \hat{\mathbf{P}}. \tag{A1}$$

Without loss of generality, we can rotate so that $\mathbf{P}$ is aligned with the z-axis and $\mathbf{p}_\perp$ is aligned with the x-axis. The two initial lab frame momenta are

$$\mathbf{p}_1 = \mathbf{P}/2 + \mathbf{p}_{||} + \mathbf{p}_\perp,$$
$$\mathbf{p}_2 = \mathbf{P}/2 - \mathbf{p}_{||} - \mathbf{p}_\perp. \tag{A2}$$

For the final state of the two-neutrino system, we need to enforce momentum conservation and energy conservation. The energy of the initial state is

$$\begin{aligned} E_{init} &= |\mathbf{p}_1| + |\mathbf{p}_2| \\ &= \sqrt{(\mathbf{P}/2 + p_{||})^2 + p_\perp^2} \\ &\quad + \sqrt{(\mathbf{P}/2 - p_{||})^2 + p_\perp^2}. \end{aligned} \tag{A3}$$

The energy of the final state is written similarly in terms of final-state parallel and perpendicular momenta $\mathbf{p'}_{||}$ and $\mathbf{p'}_\perp$. Since the contribution of $\mathbf{p'}_\perp$ to the energy is positive, the maximum magnitude of $\mathbf{p}_{||}$ is found by solving $E_{\rm fin} = E_{init}$ for $\mathbf{p'}_\perp = 0$. Similarly, the maximum magnitude of $\mathbf{p}_\perp$ is obtained when $\mathbf{p'}_\perp = 0$. These equations yield

$$p'_{\max,||} = E_{init}/2,$$
$$p'_{\max,\perp} = \sqrt{(E_{init}^2 - 2(\mathbf{P}/2)^2}. \tag{A4}$$

We show a specific example of the impact of the energy-conserving delta function in Fig. 2. The momenta of the two initial particles are shown as the two large dots, and the lines represent all possible final states that conserve two-neutrino energy and momenta.

If we call these maximum magnitudes $p_{\max,||}$ and $p_{\max,\perp}$, respectively, we can compute the phase space integral as

$$\begin{aligned} PS &= \int d^3\mathbf{q}\,\delta(E_{\rm final} - E_{init}) \\ &= (2\pi)0.785\, p_{\max,||}\, p_{\max,\perp}, \end{aligned} \tag{A5}$$

where the 2π comes from the azimuthal symmetry, the two maximum momenta can be calculated from the initial momenta, and the 0.785 comes from a numerical integration of the energy-conserving delta function. The units are energy, or momentum, squared, as expected for massless particles. We have used a short-range interaction where the matrix element is independent of the magnitude of the momentum transfer squared.

In the semiclassical approximation, we enforce energy conservation after each neutrino-neutrino vertex.

The total rate for two neutrinos can be obtained by summing over final states of the pair imposing energy conservation,

$$\begin{aligned} \text{Rate} &= \frac{2\pi}{\hbar c}\sum_{f,x,q} |\langle H_{fi}\rangle|^2 \delta(E_f - E_i) \\ &= \frac{2\pi}{\hbar c}\frac{V}{(2\pi\hbar c)^3}\int d^3\mathbf{q}\,|\langle H_{fi}\rangle|^2 \delta(E_f - E_i) \\ &= \frac{V}{4\pi^2(\hbar c)^4}\int d^3\mathbf{q}\left[\sum_{f,x}|\langle H_{fi}\rangle|^2\right]\delta(E_f - E_i), \end{aligned} \tag{A6}$$

but then we approximate

$$\sum_{f,x}|\langle H_{fi}\rangle|^2 \approx \left[(\hbar c)^3\frac{\sqrt{2}G_F}{V}\right]^2, \tag{A7}$$

and then the final expression for the rate looks like

$$\begin{aligned} \text{Rate} &= \frac{V}{4\pi^2(\hbar c)^4}\frac{(\hbar c)^6 2G_F^2}{V^2}\int d^3\mathbf{q}\,\delta(E_f - E_i) \\ &= \frac{(\hbar c)^2 G_F^2}{2\pi^2}\frac{\rho}{N}PS. \end{aligned} \tag{A8}$$

For two neutrinos the cross section can be obtained from the matrix element squared by including both the energy-conserving delta function and the relativistic "Moller" flux factor [73,74].

APPENDIX B: RANDOM SWAPS

Here we want to show that if we take a neutrino system and we apply random SWAP operations to them, the system will reach equilibrium in the one-body observables exponentially fast with a rate which is independent of the size N of the system.

The evolution is as follows: at every time step we pick a pair of neutrinos (i, j) at random and apply the operation P_{ij} to the state—this process is then repeated for L layers. The idea is to perform the calculation in the Heisenberg picture and evolve the observable instead of the state. We define equilibration once the individual flavor observables $\langle Z_i(t)\rangle$ are all equal to their average $Z_{av} = \frac{1}{N}\sum_i\langle Z_i(t)\rangle = \frac{1}{N}\sum_i\langle Z_i(0)\rangle$ where the equality follows from the conservation of the total Z in the system. Since all the expectation values go to the same limit, we consider the evolution of Z_1 only. We use U_k to specify the unitary applied at layer k. After one layer we have

$$\text{Tr}[\rho_0 U_1^\dagger Z_1 U_1 \dagger] = (1-p)\langle Z_1(0)\rangle + p\langle Z_{1_1}(0)\rangle, \tag{B1}$$

where ρ_0 is the initial state, 1_1 is the label of the neutrino swapped with 1 at the first neutrino after one layer, and p is the probability to select neutrino 1 at this layer. For uniform sampling we get $p = (N-1)/\binom{N}{2} = 2/N$. If we do an average over realizations we then get

$$\mathbb{E}Tr[\rho_0 U_1^\dagger Z_1 U_1] = (1-p)\langle Z_1(0)\rangle + pZ_{av}. \quad \text{(B2)}$$

After two layers, the probability of staying in 1 is given by the probability $(1-p)^2$ of staying there for both layers plus the probability $p/\binom{N}{2}$ of jumping once and then back to 1. We then have

$$\mathbb{E}Tr[\rho_0 U_1^\dagger U_2^\dagger Z_1 U_2 U_1] = \left[(1-p)^2 + \frac{p}{\binom{N}{2}}\right]\langle Z_1(0)\rangle + \left[p^2 + 2p(1-p) - \frac{p}{\binom{N}{2}}\right] Z_{av}. \quad \text{(B3)}$$

For a large system when $\binom{N}{2} \gg 1/(1-p) \gg 1/p$ we can approximate this neglecting factors of $p/\binom{N}{2}$ [at least if the total number of layers $L \ll \binom{N}{2}$]. But then, after L layers we have

$$\mathbb{E}Tr\left[\rho_0 \left(\prod_{k=1}^{L} U_k^\dagger\right) Z_1 \left(\prod_{k=L}^{1} U_k\right)\right] = (1-p)^L \langle Z_1(0)\rangle + [1-(1-p)^L] Z_{av}. \quad \text{(B4)}$$

But then this means that

$$\Delta_L = \mathbb{E}Tr\left[\rho_0 \left(\prod_{k=1}^{L} U_k^\dagger\right) Z_1 \left(\prod_{k=L}^{1} U_k\right)\right] - Z_{av} = (1-p)^L[\langle Z_1(0)\rangle - Z_{av}], \quad \text{(B5)}$$

which we can bound as

$$|\Delta_L| < 2(1-p)^L = 2\left(1 - \frac{2}{N}\right)^L. \quad \text{(B6)}$$

But then, the number of layers required to converge to a flavor expectation value, on each individual neutrino, which is on average at most δ away from the average Z_{av}, is at most

$$L_{eq} = -\frac{\log(1/\delta)}{\log(1-p)} \gtrsim p \log\left(\frac{2}{\delta}\right) = \frac{N}{2}\log\left(\frac{2}{\delta}\right). \quad \text{(B7)}$$

To connect this with a timescale, we assume $H = (\mu/N)\sum_{i<j} c_{ij} P_{ij}$ with coupling constants $c_{ij} \geq 0$ sampled from some distribution. The incremental time step $\Delta\tau$ at every layer is sampled from the shortest collision time on all the pairs. Its average value over different runs is then

$$\mathbb{E}[\Delta\tau] = \frac{N}{\mu \sum_{i<j} c_{ij}}, \quad \text{(B8)}$$

and if we average this over the choices of coupling constants (i.e., sampling one random set for each run and keeping them for the L layers) gives

$$\mathbb{E}_C\mathbb{E}[\Delta\tau] = \mathbb{E}_C\left[\frac{N}{\mu\sum_{i<j} c_{ij}}\right] \geq \frac{N}{\mu \mathbb{E}_C[\sum_{i<j} c_{ij}]}. \quad \text{(B9)}$$

The expectation value on the coupling constants can be performed as follows (see also [34,61]):

$$\mathbb{E}_C\left[\sum_{i<j} c_{ij}\right] = \sum_{i<j} \mathbb{E}_C[c_{ij}] = \sum_{i<j} \mathbb{E}_C[1 - \hat{\mathbf{k}}_i \cdot \hat{\mathbf{k}}_j] = \binom{N}{2} - \sum_{i<j} \mathbb{E}_C[\hat{\mathbf{k}}_i \cdot \hat{\mathbf{k}}_j]. \quad \text{(B10)}$$

The second term can be further rewritten as

$$\sum_{i<j} \mathbb{E}_C[\hat{\mathbf{k}}_i \cdot \hat{\mathbf{k}}_j] = \sum_{i<j} \mathbb{E}_C[\hat{\mathbf{k}}_i] \cdot \mathbb{E}_C[\hat{\mathbf{k}}_j] = \binom{N}{2} \mathbb{E}_C[\hat{\mathbf{k}}]^2, \quad \text{(B11)}$$

since the momenta of different neutrinos are independent of each other. For momentum direction distributed uniformly these averages are equal to zero. In the case instead of momentum directions sampled on a forward semisphere, as done in the main text, these are given instead by

$$\mathbb{E}_C[\hat{\mathbf{k}}] = \left(0, 0, \frac{1}{2}\right). \quad \text{(B12)}$$

This then directly gives

$$\mathbb{E}_C\left[\sum_{i<j} c_{ij}\right] = \binom{N}{2}\frac{4-x}{4}, \quad \text{(B13)}$$

where $x = 0$ for the uniform case and $x = 1$ for the forward hemisphere distribution instead.

The expected equilibration time is then bounded as

$$T_{eq} = L_{eq}\mathbb{E}_C\mathbb{E}[\Delta\tau] \gtrsim \frac{1}{\mu}\frac{4}{4-x}\frac{N}{N-1}\log\left(\frac{2}{\delta}\right). \quad \text{(B14)}$$

Of course this is completely independent on what the initial state was.

[1] L. Wolfenstein, Phys. Rev. D **17**, 2369 (1978).
[2] S. Mikheyev and A. Smirnov, Prog. Part. Nucl. Phys. **23**, 41 (1989).
[3] J. Pantaleone, Phys. Lett. B **287**, 128 (1992).
[4] J. Pantaleone, Phys. Rev. D **46**, 510 (1992).
[5] Y. Z. Qian and G. M. Fuller, Phys. Rev. D **51**, 1479 (1995).
[6] S. Pastor, G. Raffelt, and D. V. Semikoz, Phys. Rev. D **65**, 053011 (2002).
[7] H. Duan, G. M. Fuller, and Y.-Z. Qian, Phys. Rev. D **74**, 123004 (2006).
[8] H. Duan, G. M. Fuller, and Y.-Z. Qian, Annu. Rev. Nucl. Part. Sci. **60**, 569 (2010).
[9] S. Chakraborty, R. Hansen, I. Izaguirre, and G. Raffelt, Nucl. Phys. **B908**, 366 (2016).
[10] M. C. Volpe, Rev. Mod. Phys. **96**, 025004 (2024).
[11] N. F. Bell, A. A. Rawlinson, and R. F. Sawyer, Phys. Lett. B **573**, 86 (2003).
[12] A. Friedland and C. Lunardini, Phys. Rev. D **68**, 013007 (2003).
[13] A. Friedland and C. Lunardini, J. High Energy Phys. 10 (2003) 043.
[14] A. Friedland, B. H. J. McKellar, and I. Okuniewicz, Phys. Rev. D **73**, 093002 (2006).
[15] B. H. J. McKellar, I. Okuniewicz, and J. Quach, Phys. Rev. D **80**, 013011 (2009).
[16] A. Balantekin and Y. Pehlivan, J. Phys. G **34**, 47 (2007).
[17] Y. Pehlivan, A. B. Balantekin, T. Kajino, and T. Yoshida, Phys. Rev. D **84**, 065008 (2011).
[18] Y. Pehlivan, A. B. Balantekin, and T. Kajino, Phys. Rev. D **90**, 065011 (2014).
[19] S. Birol, Y. Pehlivan, A. Balantekin, and T. Kajino, Phys. Rev. D **98**, 083002 (2018).
[20] A. V. Patwardhan, M. J. Cervia, and A. Baha Balantekin, Phys. Rev. D **99**, 123013 (2019).
[21] M. J. Cervia, A. V. Patwardhan, A. B. Balantekin, t. S. N. Coppersmith, and C. W. Johnson, Phys. Rev. D **100**, 083001 (2019).
[22] E. Rrapaj, Phys. Rev. C **101**, 065805 (2020).
[23] A. Roggero, Phys. Rev. D **104**, 103016 (2021).
[24] A. Roggero, Phys. Rev. D **104**, 123023 (2021).
[25] Z. Xiong, Phys. Rev. D **105**, 103002 (2022).
[26] J. D. Martin, A. Roggero, H. Duan, J. Carlson, and V. Cirigliano, Phys. Rev. D **105**, 083020 (2022).
[27] A. V. Patwardhan, M. J. Cervia, and A. B. Balantekin, Phys. Rev. D **104**, 123035 (2021).
[28] A. Roggero, E. Rrapaj, and Z. Xiong, Phys. Rev. D **106**, 043022 (2022).
[29] M. J. Cervia, P. Siwach, A. V. Patwardhan, A. B. Balantekin, S. N. Coppersmith, and C. W. Johnson, Phys. Rev. D **105**, 123025 (2022).
[30] M. Illa and M. J. Savage, Phys. Rev. Lett. **130**, 221003 (2023).
[31] D. Lacroix, A. B. Balantekin, M. J. Cervia, A. V. Patwardhan, and P. Siwach, Phys. Rev. D **106**, 123006 (2022).
[32] P. Siwach, A. M. Suliga, and A. B. Balantekin, Phys. Rev. D **107**, 023019 (2023).
[33] R. Bhaskar, A. Roggero, and M. J. Savage, Phys. Rev. C **110**, 045801 (2024).
[34] J. D. Martin, D. Neill, A. Roggero, H. Duan, and J. Carlson, Phys. Rev. D **108**, 123010 (2023).
[35] J. D. Martin, A. Roggero, H. Duan, and J. Carlson, arXiv:2301.07049.
[36] A. Kost, L. Johns, and H. Duan, Phys. Rev. D **109**, 103037 (2024).
[37] D. Lacroix, A. Bauge, B. Yilmaz, M. Mangin-Brinet, A. Roggero, and A. B. Balantekin, Phys. Rev. D **110**, 103027 (2024).
[38] V. Cirigliano, S. Sen, and Y. Yamauchi, Phys. Rev. D **110**, 123028 (2024).
[39] Z. Laraib and S. Richers, Phys. Rev. D **112**, L101304 (2025).
[40] I. Chernyshev, C. E. P. Robin, and M. J. Savage, Phys. Rev. Res. **7**, 023228 (2025).
[41] M. Mangin-Brinet, A. Bauge, and D. Lacroix, Phys. Rev. D **113**, 036026 (2026).
[42] B. Hall, A. Roggero, A. Baroni, and J. Carlson, Phys. Rev. D **104**, 063009 (2021).
[43] K. Yeter-Aydeniz, S. Bangar, G. Siopsis, and R. C. Pooser, Quantum Inf. Process. **21**, 84 (2022).
[44] M. Illa and M. J. Savage, Phys. Rev. A **106**, 052605 (2022).
[45] V. Amitrano, A. Roggero, P. Luchi, F. Turro, L. Vespucci, and F. Pederiva, Phys. Rev. D **107**, 023007 (2023).
[46] P. Siwach, K. Harrison, and A. B. Balantekin, Phys. Rev. D **108**, 083039 (2023).
[47] F. Turro, I. A. Chernyshev, R. Bhaskar, and M. Illa, Phys. Rev. D **111**, 043038 (2025).
[48] I. A. Chernyshev, Phys. Rev. D **111**, 043017 (2025).
[49] L. Spagnoli, N. Goss, A. Roggero, E. Rrapaj, M. J. Cervia, A. V. Patwardhan, R. K. Naik, A. B. Balantekin, E. Younis, D. I. Santiago, I. Siddiqi, and S. Aldaihan, Phys. Rev. D **111**, 103054 (2025).
[50] O. Kiss, I. Tavernelli, F. Tacchino, D. Lacroix, and A. Roggero, Commun. Phys. **9**, 282 (2026).
[51] J. Froustey, E. Rrapaj, Y. Liu, G. Li, C. Iancu, and V. Cirigliano, arXiv:2606.12404.
[52] J. D. Martin, D. Neill, A. Roggero, H. Duan, and J. Carlson, Phys. Rev. D **108**, 123010 (2023).
[53] B. Pontecorvo, Sov. Phys. JETP **6**, 429 (1958).
[54] Z. Maki, M. Nakagawa, and S. Sakata, Prog. Theor. Phys. **28**, 870 (1962).
[55] J. E. Hirsch, R. L. Sugar, D. J. Scalapino, and R. Blankenbecler, Phys. Rev. B **26**, 5033 (1982).
[56] A. W. Sandvik and J. Kurkijärvi, Phys. Rev. B **43**, 5950 (1991).
[57] A. L. Fetter and J. D. Walecka, *Quantum Theory of Many-Particle Systems* (McGraw-Hill, Boston, 1971).
[58] N. Margolus and L. B. Levitin, Physica D (Amsterdam) **120**, 188 (1998).
[59] S. Deffner and S. Campbell, J. Phys. A **50**, 453001 (2017).
[60] F. Campaioli, F. A. Pollock, F. C. Binder, and K. Modi, Phys. Rev. Lett. **120**, 060409 (2018).
[61] D. Neill, H. Liu, J. Martin, and A. Roggero, Phys. Rev. Res. **7**, 023157 (2025).
[62] G. Martirosyan, M. Gazo, J. Etrych, S. M. Fischer, S. J. Morris, C. J. Ho, C. Eigen, and Z. Hadzibabic, Nature (London) **647**, 608 (2025).
[63] M. P. Fisher, V. Khemani, A. Nahum, and S. Vijay, Annu. Rev. Condens. Matter Phys. **14**, 335 (2023).

[64] W. Brown and O. Fawzi, arXiv:1210.6644.
[65] J. P. Kneller, G. C. McLaughlin, and J. Brockman, Phys. Rev. D **77**, 045023 (2008).
[66] H. Duan, G. M. Fuller, J. Carlson, and Y.-Z. Qian, Phys. Rev. Lett. **100**, 021101 (2008).
[67] J. Carlson, A. Roggero, and D. Neill, Data for "neutrino flavor evolution in high-flux astrophysical environments," 10.5281/zenodo.20133077, 2026.
[68] Y. Qiu, D. Radice, S. Richers, and M. Bhattacharyya, Phys. Rev. Lett. **135**, 091401 (2025).
[69] T. Wang and A. Burrows, arXiv:2503.04896.
[70] T. Wang, H. Nagakura, L. Johns, and A. Burrows, Phys. Rev. D **112**, 063039 (2025).
[71] T. Wang and A. Burrows, Astrophys. J. **997**, 325 (2026).
[72] A. Capanema, Y. Porto, and M. M. Saez, Phys. Rev. D **111**, 103021 (2025).
[73] O. Nachtmann, *Elementary Particle Physics: Concepts and Phenomena* (1990).
[74] R. Hagedorn, Selected Topics on Scattering Theory: Part 1 Relativistic Kinematics and Precession of Polarization, Technical Report (CERN, 1962).